

Additively Manufactured Winding Design for Thermal Improvement of an Oil-cooled Axial Flux Permanent Magnet Machine

Hui Tan, Xinggang Fan, *Member, IEEE*, Dawei Li, *Senior Member, IEEE*, Tianjie Zou, *Member, IEEE*, Wubin Kong, Runyu Wang, *Student Member, IEEE*, Xiaoxue Chen, and Ronghai Qu, *Fellow, IEEE*

Abstract—This article proposes a new additively manufactured winding with integrated heat sinks to improve thermal performance of an oil-cooled yokeless and segmented armature (YASA) axial flux permanent magnet machines. The heat sinks featuring pin-fin structure are integrated to the two sides and top of the winding to increase the heat transfer area and convective heat transfer coefficient, thus improving the thermal performance. Computational fluid dynamics is employed to evaluate the thermal performance of the proposed winding, which is further compared with that of the state-of-the-art rectangular winding. Besides, the influence of pin spacing in streamwise direction, tilt angle, flow rate and resistances on the thermal performance and pressure drops of the proposed winding are investigated. Finally, prototypes of the proposed winding and the counterpart rectangular winding are manufactured to verify the numerical analyses. The experimental results show that the winding temperature of the proposed winding can be reduced by 27.6 °C compared with that of rectangular winding.

Index Terms—Additive manufacturing, cooling design, oil cooling, yokeless and segmented armature axial flux permanent magnet machines.

I. INTRODUCTION

ELECTRIFICATION is a main enabler for decarbonised transportation. To achieve the “Net Zero” target in future decades [1], ambitious roadmaps have been drawn up globally, which translate into step-change performance requirements for electrical machines in terms of their power density level, from 8 kW/L to 30kW/L [2-3]. The power density of state-of-the-art machines is primarily limited

by the ability to minimize power losses and maximize heat-transfer to maintain operation within the material property boundaries. In recent years, the axial flux permanent magnet (AFPM) machines have drawn ever increasing attentions in transportation sector due to their inherent high torque density and high efficiency [4]-[6]. Among AFPM machines, the yokeless and segmented armature (YASA) AFPM machines have been the research hotspots due to their superior power density and more efficient active material utilization [7], [8]. Meanwhile, this “multi-plate” arrangement brings significant challenges in thermal management of the machine. The stator segments of YASA AFPM machines are between the two rotors without a common yoke structure as heat dissipation channel. This also leads to additional difficulty in integrated cooling system design, thus becoming a key barrier in further boosting power density of YASA AFPM machines.

To enhance the thermal performance of YASA AFPM machines, the well adopted cooling methods include air cooling [9]-[12], water cooling [13]-[15] and oil cooling [16]-[18]. Air cooling is beneficial for its low cost, simplicity and high reliability. Based on the unique segment stator structure, fins can be inserted to the space between the adjacent coils or at the coil ends to improve the thermal performance [11], [12]. Even though the thermal performance is improved by using these novel structures for the air-cooled machines, it still cannot meet the power density requirement for some applications. To further improve the cooling performance, the more efficient water cooling methods can be used [19]. Chen *et al.* applied a water jacket in contact with the inner ring of the winding [13] while Zhang *et al.* arranged some water pipes at the outer ring of the winding [14]. These techniques are supposed to achieve limited thermal performance improvement due to the insufficient heat dissipation area. In order to further strengthen the cooling performance, Chang *et al.* [15] applied U-shape water-cooling pipes which are integrated insides the fins around the segment coils to reduce the thermal resistance. It is reported the power density has been improved by 38% using this method. Compared with water cooling, oil cooling is a more effective cooling option, as oil can be in direct contact with windings to transfer heat much more efficiently without concerns in degrading insulation level [20]. Hence, direct oil cooling attracts more attention in ultra-high power density applications [16]-[18]. Camilleri *et al.* proposed a compact and integrated stator oil-immersed cooling structure for a YASA AFPM machine with peak power density of 6.7 kW/kg [17]. Besides, they further integrated a heat sink with the coil, which reduces the maximum winding temperature by 87 °C and increases current

This work was supported in part by the National Natural Science Foundation of China under No. 52007069, the National Natural Science Foundation of China under Grant 51991382 and the Maritime Technology Innovation Center Foundation of China under Grant JJ-2020-712-01.

Hui Tan is with the China-EU Institute for Clean and Renewable Energy, Huazhong University of Science and Technology, China (e-mail: tanhuitongxue@163.com).

Xinggang Fan, Dawei Li, Wubin Kong, Runyu Wang, and Ronghai Qu are with the State Key Laboratory of Advanced Electromagnetic Engineering and Technology, Huazhong University of Science and Technology, China (e-mail: xinggangfan@hust.edu.cn; daweil@hust.edu.cn; wbkong@hust.edu.cn; runyuwang@hust.edu.cn; ronghaiqu@hust.edu.cn).

Tianjie Zou is with the Power Electronics, Machines and Control (PEMC) Group, University of Nottingham, NG7 2RD, Nottingham, UK (e-mail: Tianjie.Zou@nottingham.ac.uk).

Xiaoxue Chen is with the State grid wuhan electric power supply company, China (e-mail: chenxx30@hb.sgcc.com.cn).

density by 140% compared with traditional structure [18]. The work has shown great potential in improving the thermal performance using novel winding cooling structure, whereas this structure is difficult to manufacture, which has limited its applicability.

In order to enhance the thermal performance of machines while overcoming manufacturing problems, additive manufacturing (AM) technology offers great possibilities [21]-[23]. Based on the AM technology, complicated structures with advanced designs of machine components, such as windings [24]-[27] and permanent magnets [28], [29], can be manufactured in a highly flexible and customized way. Among them, the AM winding attracts more attention in terms of their great potential in improving the slot filling factor [24] and thermal performance [25]-[27]. Some researches have already been carried out to improving the thermal performance for the radial-flux machines using AM technology [30], [31]. For the YASA AFPM machines with special structure and cooling configuration, the capability of AM technology in improving the thermal performance remains to be further investigated.

In this paper, a new additively manufactured winding with integrated heat sinks is proposed to improve the thermal performance for a YASA AFPM machine, which is configured with a unique oil cooling structure. The heat sinks are featured with pin-fin structure and are integrated on the winding surface, which can extremely increase the heat dissipation area and stir up fluid turbulence, thus improving the thermal performance. The remaining content of this paper is structured as follows. The studied oil-cooled YASA AFPM machines and the proposed winding structure will be introduced in detail in Section II. In Section III, computational fluid dynamics (CFD) models of the proposed winding and the rectangular winding are established. Besides, the thermal performance and flow condition of the proposed winding and the rectangular winding will be detailly investigated and analyzed. In addition, the influence of pin spacing in streamwise direction, tilt angle, flow rate and resistances on the thermal performance of the proposed winding are studied. In Section IV, the experimental validation of the proposed winding and CFD model will be presented and discussed. Finally, Section V concludes this article.

II. PROPOSED WINDING STRUCTURE WITH INTEGRATED PIN-FIN HEAT SINKS

A. Structure and Parameters of Studied YASA AFPM Machine

In this section, the structure and parameters of the studied YASA AFPM machine with a unique cooling structure will be introduced. The main parameters are shown in Table I. The studied machine is targeted for aerospace propulsion applications with a continuous power density of 4.8 kW/kg. For the studied machine, the stator is between the two rotors, which makes it difficult to dissipate the high winding losses to the ambient. Since the main losses are located in the stator, the power density will be limited if the stator cooling is not sufficient.

TABLE I

MAIN PARAMETERS OF THE STUDIED MACHINE	
Machine Parameters	Value
Rated power	120 kW
Rated speed	3000 rpm
Rated torque	382 Nm
Rated current	220 A
Rated current density	33.5 A/mm ²
Number of poles	20
Number of slots	24
Physical air gap	2 mm
Stator axial length	33 mm
Active outer diameter	300 mm
Active inner diameter	208 mm
Magnet thickness	9 mm
Turns per coil	25
Number of parallel branches	4
DC bus voltage	400V

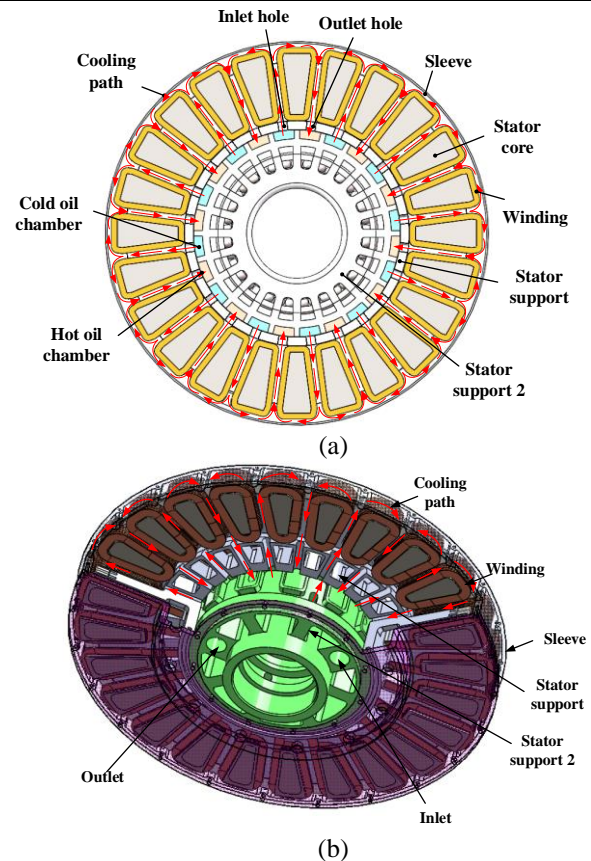


Fig. 1. Cooling structure of the studied YASA AFPM machine. (a) Cross section of the oil-cooled stator. (b) Structure of the oil-cooled stator.

To improve the stator cooling, a unique stator-immersed oil cooling structure is proposed as shown in Fig.1. The cooling structure is designed based on the special mechanical support, which fixes 24 coils along the stator circumference. Oil first enters into the cold oil chamber from an external inlet and then is distributed to the stator chamber through 12 internal inlet holes. After the oil flows into the stator chamber, it flows radially between the adjacent coils and flows circumferentially on the top of the coil to absorb the stator losses. Then, it gathers with the oil from the adjacent branch and flows between the adjacent coils to further absorb the heat. After that, it flows out through 12 internal outlet holes, which are alternately arranged with the 12 internal inlet holes, and finally collects in the hot oil chamber and flows out through an

external outlet. The proposed cooling structure integrates with the active magnetic components and the mechanical parts, which makes it much compact and lightweight. Besides, the direct contact with the oil and stator support also greatly reduces the thermal resistance between the winding and coolant, thus significantly improving the thermal performance.

B. Proposed Winding Structure with Integrated Pin-fin Heat Sinks

Based on the proposed cooling structure, a new winding structure adopting AM technology is proposed to further improve the thermal performance from the point of view of winding design as shown in Fig.2. To improve the thermal performance of winding, staggered and cylinder pin-fin heat sinks (PFHS) with 5.5mm spacing are added to the two sides and top of the winding (as shown in Fig.2 (b)). The pin-fin diameter is equal to the axial thickness of each turn (0.81mm) and height is maximum to almost hit the adjacent winding and sleeve. As there are four stator support cylinders to fix the coil, only 11 turns in the middle are configured with PFHS in both sides as a practical consideration. Each turn has 7 or 8 layers of pin-fins on each side which are 45° tilt upward considering the processability of AM technology. At the top of the winding, apart from the two turns at both ends, each turn has 6 or 7 staggered PFHS which are vertically upward. Besides, winding cross-section area is increased as much as possible to decrease the coil resistance by utilizing the space at the corners, as shown in the blue circle of Fig.2 (a). The windings are assembled with the other parts as shown in Fig.2 (c). The stator shoes made of SMC are used to reduce the slot opening while fixing the coil. Based on the above designs, heat dissipation area can be significantly increased and the turbulence intensity can be enhanced due to the extended pin-fins, thus improving the thermal performance.

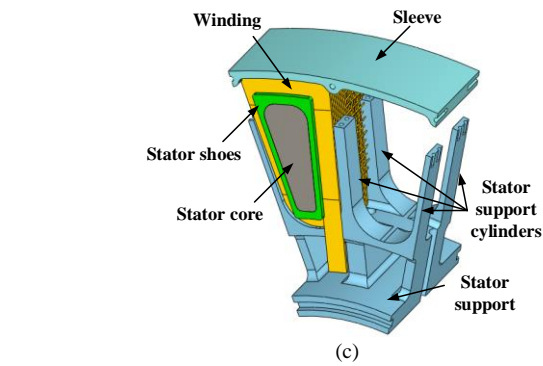
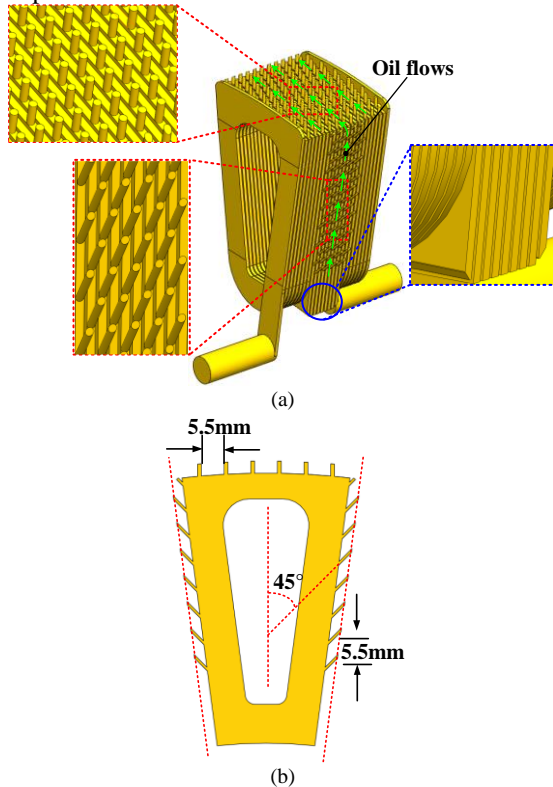


Fig. 2. (a) Proposed winding structure. (b) Cross section of the proposed winding. (c) Stator assembly.

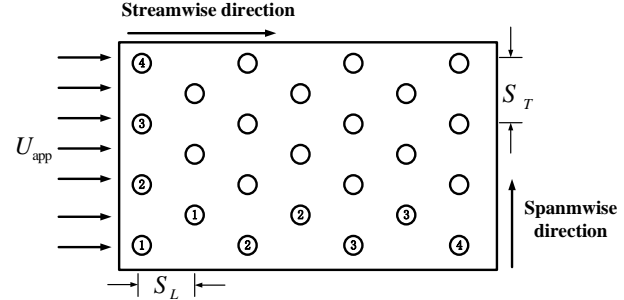


Fig. 3. Parameters of staggered pin-fin array.

The PFHS have been widely used in the cooling of electronic components [32], [33]. For the pin-fin structure, the heat transfer coefficient h_{fin} can be calculated by dimensionless number as following [34]

$$Nu_d = \frac{h_{fin} d}{k_f} = C_1 Re_d^{1/2} Pr^{1/3} \quad (1)$$

where C_1 is a constant which depends on the longitudinal and transvers spacing, array of the pins, and thermal boundary conditions. Nu_d is Nusselt number of PFHS, k_f is thermal conductivity of PFHS. Re_d is Reynold number of PFHS. Pr is Prandtl number.

$$C_1 = \frac{0.61 S_T^{0.591} S_L^{0.053}}{(S_T - 1)^{0.5} [1 - 2 \exp(-1.09 S_T)]} \quad \text{Staggered} \quad (2)$$

$$C_1 = \frac{[0.2 + \exp(-0.55 S_T)] S_T^{0.785} S_L^{0.212}}{(S_T - 1)^{0.5}} \quad \text{In-line} \quad (3)$$

where S_L is pin spacing in streamwise direction. S_T is pin spacing in spanwise direction.

Based on the above formulas, the relationship between thermal resistance and fluid velocity is shown as Fig.4. It can be seen that the thermal resistance of single plate is almost 15 times that of PFHS under the same fluid velocity due to PFHS' larger heat transfer area and convective heat transfer coefficient (CHTC). Compared with in-line array, the staggered array has lower thermal resistance under the same heat transfer area. That is attributed to the fact that the flow disturbance of the staggered array is more intensive compared with that of the in-line array when fluid flows in curved channel with alternating contraction and expansion. Therefore, the thermal performance can be significantly improved by using staggered PFHS compared with single plate. It should be noted that the pin-fins also increase the pressure drops due to

the decreased flow area, increased flow velocity and local turbulence.

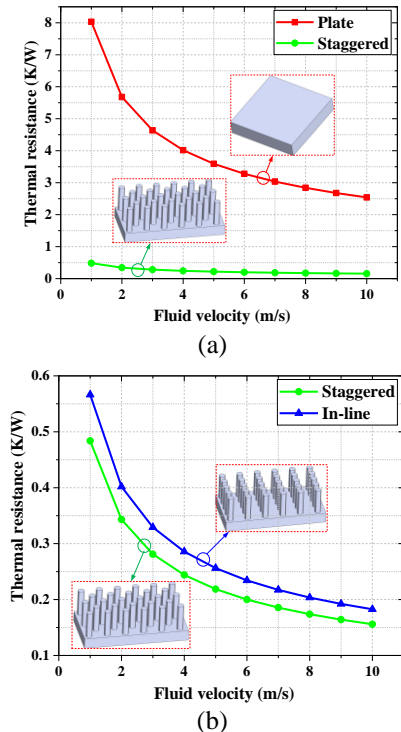


Fig. 4. Thermal resistance under different fluid velocities. (a) Plate and staggered pin-fins. (b) Staggered and in-line pin-fins.

III. CFD MODELS AND RESULTS

A. Basic Equations and CFD Models

In this section, CFD is employed to evaluate the thermal performance and flows of the proposed winding and rectangular winding. The rectangular winding in AFPM machines is proved to be superior than cylindrical winding [35]. Therefore, the proposed winding is compared with the rectangular winding manufactured by the winding mould from the flat wires to prove its superiority. The foundations of CFD are mass conservation equation, momentum conservation equation and energy conservation equation. Based on the CFD, complex geometries and fluid domains can be accurately computed.

The CFD establishes differential equations in discrete microelement and solves them using Navier-Stokes equations with high accuracy in 3-D laminar and turbulent flow. To solve complicated 3-D turbulence, Reynolds-averaged Navier-Stokes (RANS) equations as following are used to reduce computational cost [36].

$$\frac{\partial \bar{U}_i}{\partial x_i} = 0 \quad (4)$$

$$\rho \frac{\partial \bar{U}_i}{\partial t} + \rho \frac{\partial}{\partial x_j} (\bar{U}_i \bar{U}_j) = -\frac{\partial P}{\partial x_i} + \frac{\partial}{\partial x_j} (2\mu S_{ij} - \rho \overline{u'_j u'_i}) \quad (5)$$

where \bar{U} and u are fluid time-average and fluctuating velocity respectively, P is the pressure, μ is dynamic viscosity of fluid, S_{ij} is mean strain-rate tensor, $-\rho \overline{u'_j u'_i}$ is symmetric Reynolds stress tensor with six components.

Due to the complicated structure of the proposed winding, the flow characteristics are inherently complex. The fluid flows in alternating channels of contraction and expansion, leading to complicated fluid impact and separation phenomenon due to the PFHS. Therefore, the choice of turbulence model is crucial. Among the turbulence models, the high Reynolds number $k-\epsilon$ model is only valid in the fully developed flow region. In contrast, the $k-\omega$ model is more accurate in solving fluid region near the wall [37]. Based on them, the shear stress transport (SST) $k-\omega$ model combines $k-\omega$ model near wall and $k-\epsilon$ model for the free flow to get accurate results and save time [38], which has good performance for swirling flows without requiring damping and improves separation flow prediction [36]. Therefore, in these CFD models, the SST $k-\omega$ model is adopted.

The CFD model of the proposed winding with its main boundary conditions is developed as shown in Fig.5. To reduce simulation time, the full machine model is simplified and only a single pole piece (include a winding, a stator core, a stator support and two endcaps) is studied based on reasonable consideration of circumferential symmetry for the machine. Since the stator shoes aren't located on the main heat dissipation path, to reduce the manufacturing complexity of the cooling specimen, the stator shoes are not considered in this study. To simulate the temperature of winding, both solid parts and fluid domain are modeled due to conjugate heat transfer between solid parts and oil. The mass-flow-inlet boundary condition is applied to the inlet with inlet oil at 30 °C and 1.6 L/min. Moreover, the pressure-outlet boundary condition is set at the outlet with 0 Pa, which is reference for upstream pressure. With power loss of stator core neglected in the pole piece model which only carry DC current, the copper loss of the proposed winding and rectangular winding are 590.3 W and 586.3 W respectively based on the same input current (220 A) due to the different designed resistance (10.5 mΩ and 9 mΩ at room temperature). The cross-section area of the proposed winding is smaller than that of the rectangular winding due to thicker insulation (the same total axial thickness as that of rectangular winding), resulting in higher resistance.

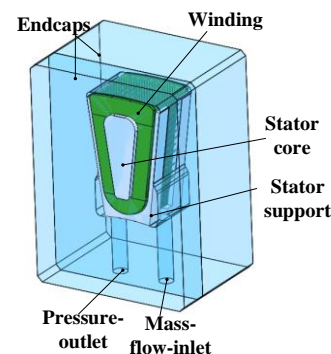


Fig. 5. The CFD model of the proposed winding.

With the winding temperature being the research focus, reasonable considerations on thermal conductivities of every component in this model, especially the winding part, are important which are directly related to thermal resistances. Since the winding is a heterogeneous body including both copper and insulation material, the modelling of winding is

complex and time-consuming, thus some equivalence is required. In the CFD model, the winding is represented by a solid constituted of compound which has different thermal conductivities in different directions as shown in Fig.6. In the actual prototypes, there is a gap between the winding and the endcaps, which is filled with epoxy to restrict the flow paths. To simplify the CFD models, the winding is directly in contact with the endcaps. To consider the heat transfer between winding and endcaps, the contact thermal resistances are added to the contact surfaces between the winding and the endcaps. In the CFD models, the contact thermal resistance is inserted by setting an equivalent epoxy gap (2 mm) on the contact surfaces between the winding and the endcaps. Using rectangular wires, slot fill can be increased and resistance can be decreased. As for the proposed winding model, based on the rectangular winding model, the PFHS are added to increase the heat transfer area and enhance turbulence to increase CHTC. As gaps between turns of winding increase the heat transfer area between winding and oil, some grooves are added to obtain more precise results. Furthermore, windings are further divided into several small parts and each part has its own local coordinate system as per their anisotropic thermal conductivities to increase the reasonability of the CFD simulation.

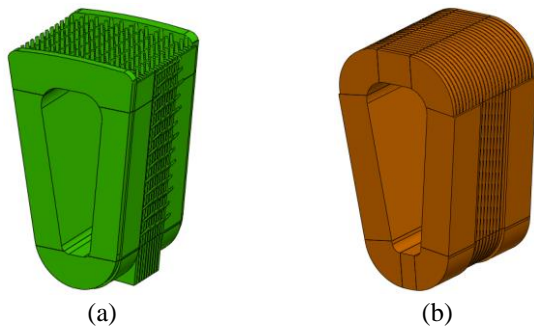


Fig. 6. (a) Proposed winding model. (b) Rectangular winding model.

TABLE II

PROPERTIES OF MATERIALS APPLIED IN THE CFD MODELS

Parts	Materials	Thermal Conductivity(W/m/°C)	Heat Capacity (J/kg/°C)	Density (kg/m ³)
Stator Core	Steel	36	460	7850
Stator support	Aluminum alloy	168	900	2790
Endcap	Polycarbonate	0.2	1256	1200

The equivalent thermal conductivity of winding can be calculated using Hashin and Shtrikman (H+S) as following [39].

$$k_e = k_i \frac{(1 + v_c)k_c + (1 - v_c)k_i}{(1 - v_c)k_c + (1 + v_c)k_i} \quad \text{Series} \quad (6)$$

$$k_e = v_c k_c + v_i k_i \quad \text{Parallel} \quad (7)$$

where k_c and k_i is thermal conductivity of copper and insulation material respectively, v_c and v_i is the volume ratio of copper and insulation material respectively. The equivalent thermal conductivities of the proposed winding and rectangular winding in tangential, radial and axial direction are 295.99/295.99/1.32 W/m/°C and 338.07/338.07/2.33 W/m/°C respectively. The detail properties of materials applied in the

CFD models are listed in Table II.

The cooling medium in the studied YASA AFPM machine is aviation lubricating oil. The relationships between oil properties and temperature are shown as Table III. As the CHTC is sensitive to oil properties, the oil properties in CFD model are adjusted to be temperature dependent function according to Table III to get more accurate results.

TABLE III

OIL PROPERTIES VARIATION WITH TEMPERATURE [°C] [37]

Properties	Expression
Density (kg/m ³)	$\rho = 983.71 - 0.70T$
Heat Capacity (J/kg/°C)	$C_p = 1946.13 + 2.75T$
Kinematic viscosity (mm ² /s)	$\nu = 154.41e^{-0.046T}$
Thermal conductivity (W/m/°C)	$\lambda_f = 0.15 - 2.99T + 4.39E - 7T^2$

In addition, high quality mesh is calculation foundation of CFD. In the CFD model, the 3D mesh is developed and optimized by Fluent Meshing. To improve mesh quality and decrease number of mesh, tetrahedral elements with minimum size set at 0.1 mm and maximum size set at 3 mm are applied in the solid domain and fluid domain due to their good adaptability in complex geometry. The skewness and aspect ratio are usually used to evaluate the quality of the 3D mesh, which are usually required below 0.95 and 15 respectively. Besides, 3-layer boundary layer mesh with growth rate of 1.1 is employed in the interfaces between solid domain and fluid domain, which is essential in complex flow condition. The value of dimensionless wall distance y^+ from the first centroid to the wall is used to measure whether inflation mesh is refined properly, which is better less than 1 in SST $k-\omega$ model and can be calculated by formulas (8) and (9).

$$v_* = \sqrt{\frac{\tau_w}{\rho}} \quad (8)$$

$$y^+ = \frac{y\rho v_*}{\mu} \quad (9)$$

where y is the distance between the mesh and the solid wall, v_* is friction velocity, τ_w is wall shear stress. The mesh of proposed winding is shown in Fig.7. A mesh-independent analysis has been done to ensure the accuracy of results, and the total number of elements in the final model is 65 million.

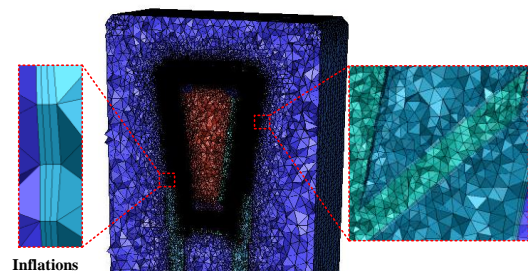


Fig. 7. Mesh of the proposed winding model.

B. Simulation results

Based on the mesh and boundary conditions mentioned in previous section, the streamline and velocity of the proposed winding and rectangular winding are shown as Fig.8. The

maximum oil velocity (2.2 m/s) of the proposed winding model is equal to that of the rectangular winding model. Compared with the proposed winding model, the maximum oil velocity of the rectangular winding model occurs at the top of winding due to drastic area contraction. As the limitation of processing capability, the rectangular winding usually features a large rounded corner when bending, which lead to reduced fluid area at the top of the rectangular winding model. Therefore, oil velocity at the top of the proposed winding model is lower than that of the rectangular winding model. In the meanwhile, the maximum oil velocity of the proposed winding model occurs at two sides of winding due to PFHS' disturbance. Besides, the oil velocity in two sides of the proposed winding is higher than that of the rectangular winding model. In addition, average oil velocity of the proposed winding model is almost the same as that of the rectangular winding. It can be seen from Fig.8 that oil flow bypasses and impacts the staggered PFHS to form severe turbulence and interactive wake in the proposed winding model. Whereas, oil flow is laminar in the rectangular winding model. Compared with laminar, turbulence has higher fluid velocity and better thermal performance under the same flow rate due to heat exchange of different fluid layers.

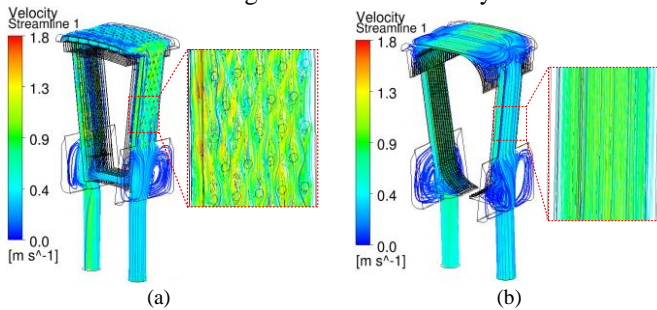


Fig. 8. Streamline. (a) Proposed winding model. (b) Rectangular winding model.

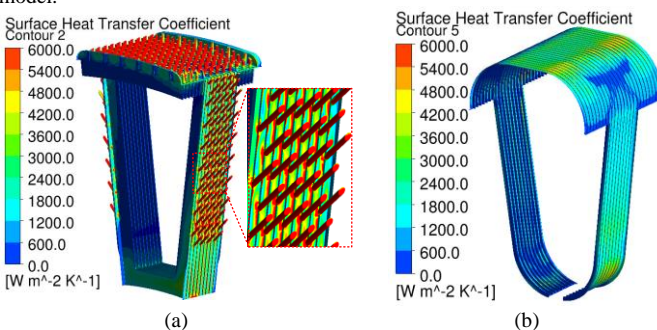


Fig. 9. Surface CHTC distribution. (a) Proposed winding model. (b) Rectangular winding model.

To further study the thermal performance of the proposed winding, the surface CHTC of the proposed winding and rectangular winding model are investigated as shown in Fig.9. It can be seen that the overall average CHTC of the proposed winding model is higher than that of the rectangular winding model. For the proposed winding model, the CHTC around PFHS is maximum and CHTC increase along fins from top to bottom. This is due to the fact that local turbulence stimulates heat transfer of different oil layers around PFHS and higher oil velocity around PFHS increases Reynolds number. For the rectangular winding model, CHTC remains almost the same in two sides of winding as the laminar oil flow and the maximum value occurs at the top of winding due to higher oil velocity.

Besides, the CHTC variation is mainly caused by area variation.

Fig.10 shows that the maximum winding temperature of the proposed winding model (78.6 °C) is decreased by 33.2 °C compared with that of the rectangular winding model (111.8 °C). For the two models, winding temperatures both increase from top to bottom of winding. The maximum winding temperature of the rectangular winding model occurs at the bottom of winding in two ends due to zero local oil flow. Whereas, the maximum winding temperature of the proposed winding model occurs near the outlet. Besides, for the proposed winding model, minimum winding temperature occurs at the top of PFHS due to the higher CHTC and heat transfer area. Compared with the proposed winding model, winding temperatures in two sides of winding are much higher in the rectangular winding model. On one hand, the PFHS of the proposed winding model provide about 1.75 times heat transfer area that of the rectangular winding model. On the other hand, PFHS induce turbulence which feature higher Reynolds number and higher CHTC.

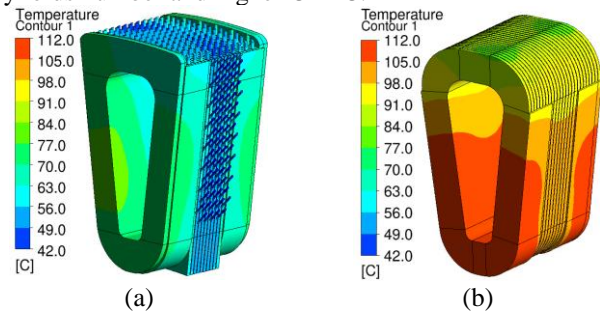


Fig. 10. Temperature distribution. (a) Proposed winding model. (b) Rectangular winding model.

The pressures drops of the two models are shown as Fig. 11. It can be seen that for the proposed winding model, the pressure drops are mainly located in channels at the winding two sides, which are mainly caused by the PFHS. Whereas, for the rectangular winding model, the pressure drops are mainly located in channels at the winding top. It is attributed that the winding top channels are smaller due to the arched shape of the winding on the top. The curvature of the arch is limited by the mechanical properties of the rectangular winding at the corners, which is not a problem if AM technology is used. In total, the pressure drop of the proposed winding (26.0 kPa) is not significantly higher (22%) than that of the rectangular winding.

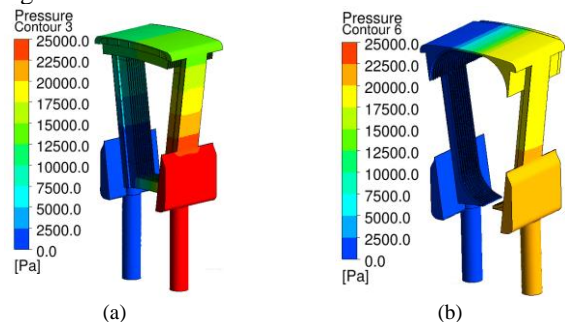


Fig. 11. Pressure drops. (a) Proposed winding model. (b) Rectangular winding model.

In summary, the main simulation results are listed in Table IV. The resistance of the proposed winding is 16.7% higher than that of rectangular winding at room temperature. Besides,

the system loss of the proposed winding is almost the same as that of rectangular winding due to lower average winding temperature. Under this condition, the maximum winding temperature of the proposed winding can be reduced by 33.2 °C compared with the rectangular winding. Meanwhile, the pressure drop is increased by 22% as a penalty.

TABLE IV
SIMULATION RESULTS

Models	Proposed winding	Rectangular winding
Rated current (A)	220	220
Current density (A/mm ²)	37.9	33.5
Flow (L/min)	1.6	1.6
Resistance (mΩ)	10.5	9
(Room temperature)		
System loss (W)	590.3	586.3
(Operating temperature)		
Maximum winding temperature (°C)	78.6	111.8
Pressure drops (kPa)	26.0	21.3

C. Effect of Parameters

Based on Equations (1)-(3), pin spacing in streamwise direction and spanwise direction and number of rows in streamwise direction all affect the thermal performance of PFHS. However, for the proposed winding structure, the pin spacing in spanwise direction is equal to the spacing between adjacent turns. Besides, the pin spacing in streamwise direction is inverse proportional to the number of rows in streamwise direction. Therefore, only the pin spacing in streamwise direction and tilt angle are investigated in this section.

The effect of the pin spacing of PFHS in streamwise direction is investigated by CFD, as shown in Fig.12. It can be seen that the temperature of winding increases while pressure drops decrease as spacing increasing. This is because the wake downstream may interact with the PFHS in the next row for intensive PFHS, which enhances the turbulence intensity. The enhanced turbulence intensity, together with the increased heat dissipation area of PFHS reduces the thermal resistance, thus decreasing winding temperature. Meanwhile, the intensive PFHS also leads to decreased flow area, increased flow velocity and local turbulence phenomena, which cause the pressure drop increasing.

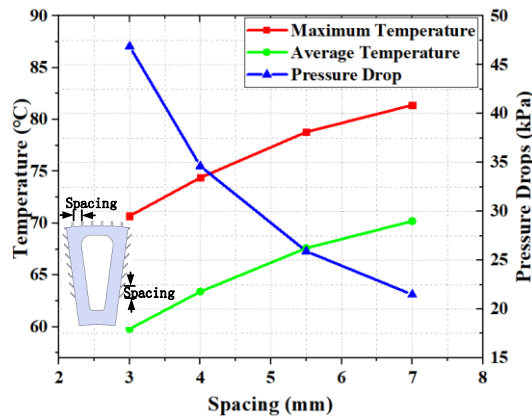


Fig. 12. Temperature and pressure drops of the proposed winding with different spacings. Note: Inlet temperature is 30 °C and flow is 1.6 L/min.

Moreover, different tilt angles are selected to study the effect on PFHS. The results are shown as Fig.13. It can be seen that the winding temperature almost does not change (less than 1%) due to the almost same heat transfer area and

heat transfer coefficient. Besides, the pressure drops increase first and then decreases with tilt angle increasing, and it reaches maximum value when tilt angle is -7.5° (perpendicular to winding). On one hand, tilt angle affects friction loss through friction loss factor. When PFHS are perpendicular with winding, the friction factor reaches maximum value. On the other hand, tilt angle also affects local loss. The local loss factor is maximum when PFHS are perpendicular with winding due to most serious fluid area variation. In total, the pressure drops are maximum when tilt angle equals to -7.5° and pressure drop curve is almost symmetry about -7.5°.

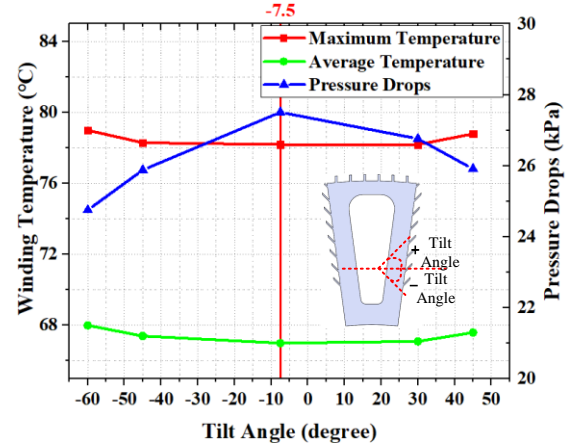


Fig. 13. Temperature and pressure drops of the proposed winding with different tilt angles. Note: Inlet temperature is 30 °C and flow is 1.6 L/min.

Process of the AM technology directly affects the resistance of the proposed winding, thus affecting the winding temperature. To investigate the influence of the process of the AM technology on the thermal performance of the proposed winding, winding temperatures based on different resistances are compared, as shown in Fig.14. It can be seen that the winding temperature of the proposed winding is sensitive to the winding resistance. The higher the resistance of the proposed winding, the higher the proposed winding temperature.

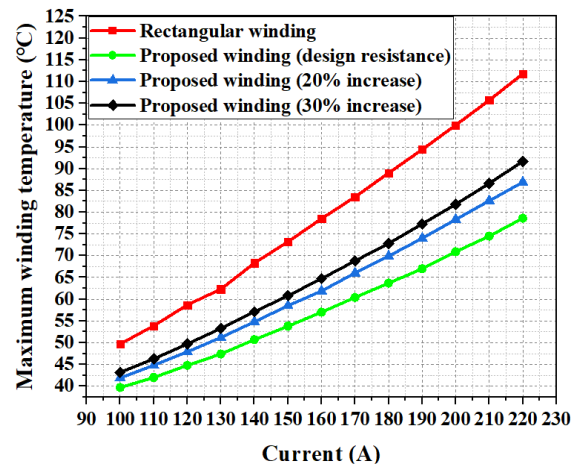


Fig. 14. Winding temperature under different resistances of the proposed winding. Note: Inlet temperature is 30 °C and flow is 1.6 L/min.

IV. EXPERIMENTAL VALIDATION AND ANALYSIS

To validate the effectiveness of the proposed winding and the CFD models, two coils including the proposed one and the conventional rectangular one are prototyped. As copper has

high reflectivity to the typically applied laser with long wavelength and has high thermal conductivity to dissipate heat quickly, it cannot absorb and accumulate enough power to melt well, which makes it difficult to manufacture using the typical laser powers by AM technology [40]. In this paper, the proposed winding is additively manufactured by Trumpf TruPrint 1000 green edition with green laser of TRUMPF as shown in Fig.15 (a).

The tested coil resistance of the proposed winding prototype is 13.24 mΩ at room temperature, which is 26% higher than the designed resistance (10.5 mΩ). The increase of resistance may be attributed that the compactness of the printed copper on the coil surface is not high and the copper on the surface got oxidized due to the unprotected processing from the oxygen, as shown in Fig. 15(a) in which the winding surface is much coarse and gets black. To ensure insulation strength, a thicker insulating layer compared to rectangular winding is required due to the coarse surface. Due to the large number of turns, the larger coil surface area also magnifies the defects of additive manufacturing. With the printing parameters and corresponding processing techniques improved, the conductivity of the printed copper can be further improved. After the printing, a high temperature insulating paint is sprayed on the surface to insulate the coil, as shown in Fig. 15(b). The insulation coating called “SCOTCHCAST BRAND ELECTRICAL Resin 260 C-free” is supplied by 3M company. The insulation powder is absorbed to the winding surface under electrostatic field. Then the winding with the insulation material is heated to solidify the insulation powder to form the insulation layer on the winding surface.

The coil prototypes are further assembled with the stator core, the support and a transparent case to form the model shown in Fig. 5, as shown in Fig. 16. Besides, two temperature sensors (PT100) are inserted into winding through slots of stator core to measure temperature of coil as shown in Fig.16 (c).

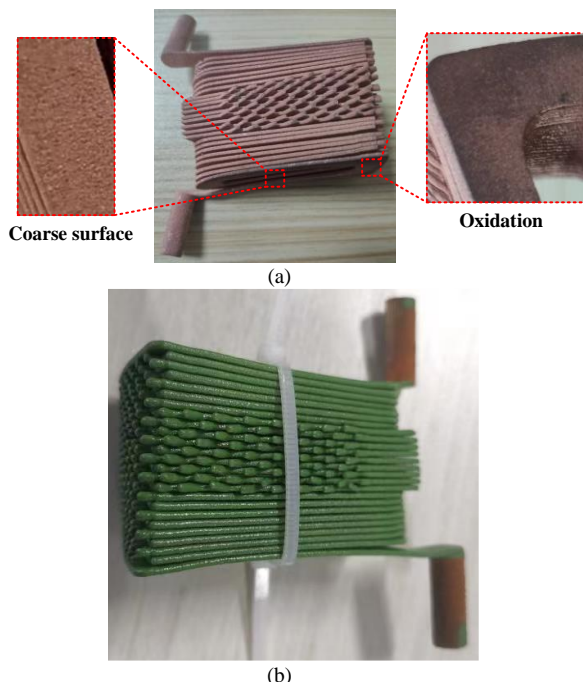


Fig. 15. The proposed winding. (a) Varnished before. (b) Varnished after.

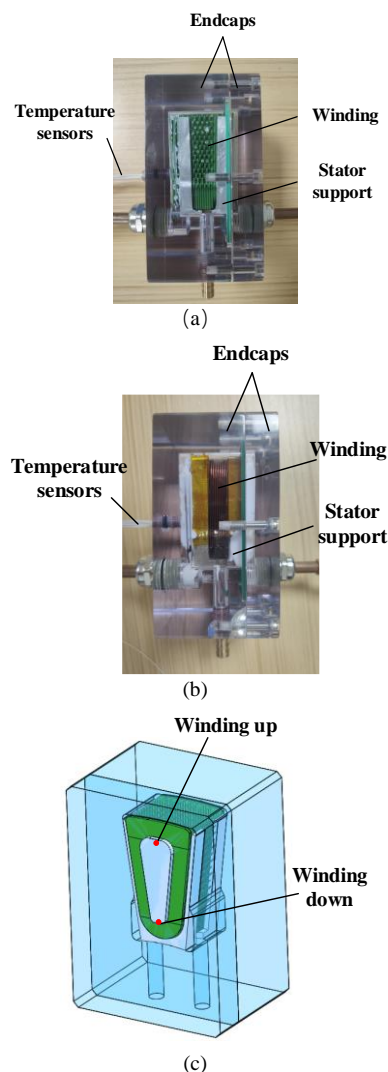


Fig. 16. (a) Proposed winding prototype. (b) Rectangular winding prototype. (c) Configuration of temperature sensors.

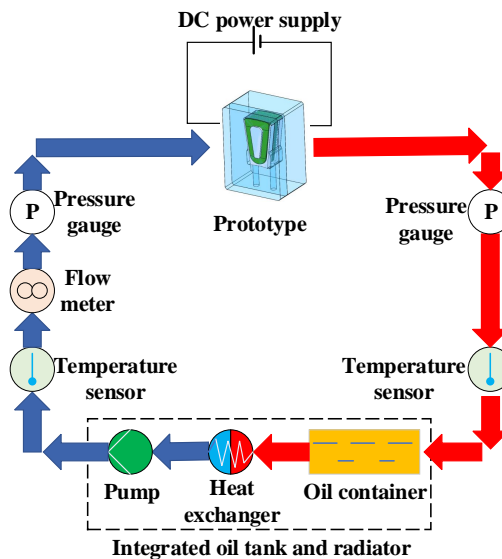


Fig. 17. Test up configuration.

The experimental setup is used to verify the thermal performance of the proposed winding as shown in Fig.17 and Fig.18. The oil flow rate can be adjusted by controlling the

variable frequency pump integrated in the integrated oil tank and radiator. The oil flow can be kept around the setting value through proportional integral (PI) feedback adjustment method. Inlet oil temperature is set at 30 °C by integrated fuel tank and radiator. Two temperature sensors (PT100) are applied to measure temperature of oil in inlet and outlet. Two pressure gauges are used to measure pressure of inlet and outlet, whose range is 0.6 MPa and accuracy is ± 3 Pa. Besides, the flow meter is located at inlet to measure flow rate of oil. DC current is injected to winding to supply winding loss by DC power supply.

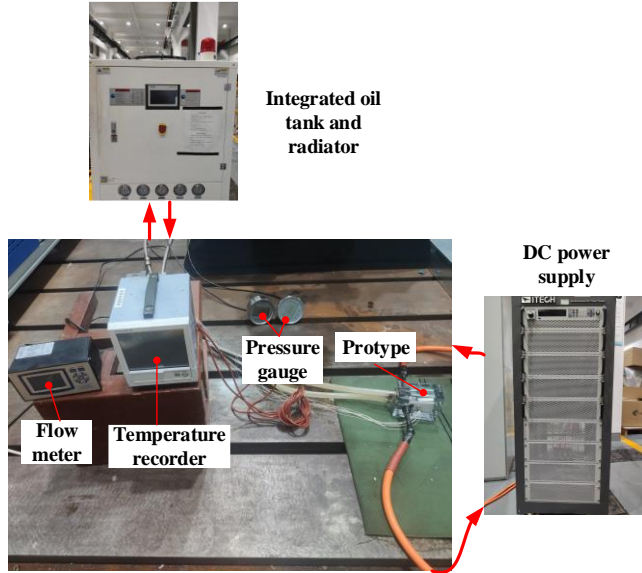


Fig. 18. Experiment platform.

The experimental results of rated condition (220 A, 1.6 L/min) are shown in Table V. Compared with the rectangular winding, the hot spot temperature (temperature of “Winding down”) of the proposed winding is reduced by 27.6 °C. At that time, the current density of the proposed winding and rectangular winding are 37.9 A/mm² and 33.5 A/mm² respectively. In addition, the hot spot temperature of the proposed winding reaches 145.7 °C under 50 A/mm² and 1.6 L/min. It can be seen that the pressure drops of the proposed winding are slightly lower than that of the rectangular winding.

TABLE V
EXPERIMENTAL RESULTS

Models	Proposed winding	Rectangular winding
Designed resistance (mΩ)	10.5	9
Teste resistance (mΩ)	13.4	9.06
Winding up (°C)	59.7	114.4
Winding down (°C)	87.9	115.5
Pressure drop (kPa)	23	30
System loss (W)	758.8	586.3

To validate the CFD models, the simulation winding temperatures under different current levels and flow rate of the proposed winding model and rectangular winding model are compared with the measure ones as shown in Fig.19. It can be seen that the simulation temperatures agree well with the measured ones. The error of the winding temperature between the experiment results and simulation results is less than 8%. The small error indicates that the CFD models are accurate to describe the thermal performance of the proposed winding and

rectangular winding. The small difference is mainly due to imprecise thermal sensors locations, inaccurate winding loss, some extra gaps in prototypes where oil flow can pass through.

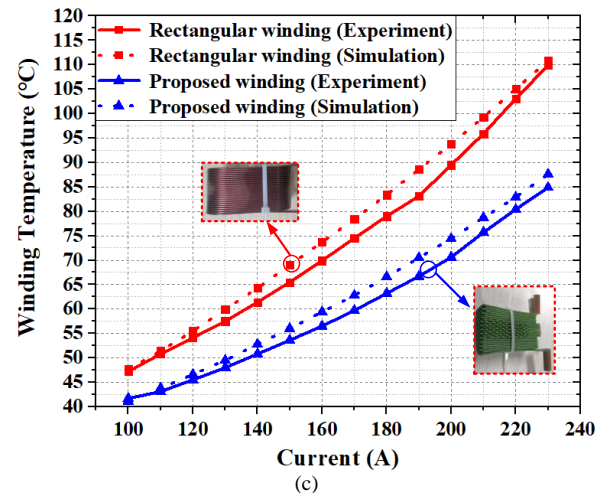
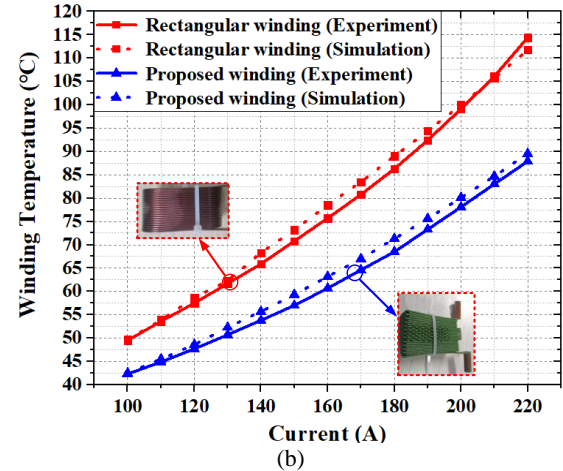
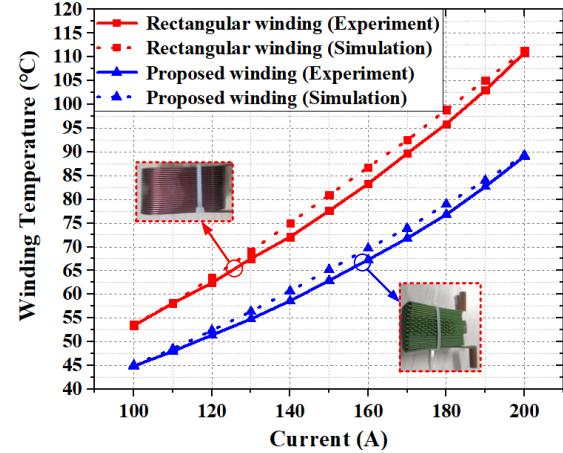


Fig. 19. Simulation results and experimental results. (a) 1.1 L/min.(b) 1.6 L/min. (c) 2.1 L/min.

Furthermore, the simulated and experimental results of pressure drops without injecting current (Inlet temperature is 30 °C) are shown as the Fig.20. It can be seen that the pressure drop of the rectangular winding is slightly higher than that of the proposed winding. When the flow rate is 1.6 L/min, the experimental pressure drop of the rectangular winding is about 9.7% higher than that of the proposed winding. The error of

the pressure drop between the experiment results and simulation results is less than 11%. The error is mainly due to CFD model simplification and measurement errors.

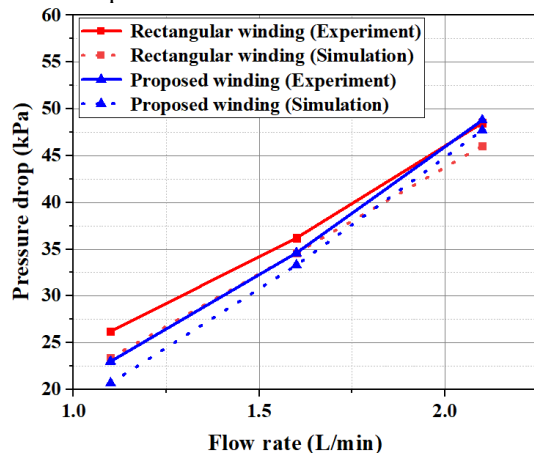


Fig. 20. Simulation results and experimental results of pressure drop without input current. Note: Inlet temperature is 30 °C.

The above analysis shows the great potential of the proposed winding concept for high power density electrical machines applied in transportation. For mass production occasions, such as electrical vehicles, the proposed AM winding may increase the production time and cost, which is rather important and have to be considered in the area. However, in some applications, such as racing cars and more electrical aircraft, where the limitation of production time and cost are looser, the AM technology can serve as a good alternative to extend the boundaries of motor output performance, thus meeting the ultimate requirements of motor output performance in these occasions.

V. CONCLUSION

This paper proposes a new winding structure using AM technology to improve the thermal performance of YASA AFPM machines. Based on a unique oil cooling structure of the studied machine, the proposed winding integrates PFHS which are located on the two sides and top of the winding to increase heat transfer area and CHTC. The flow characteristics, CHTC, pressure drop and temperature distribution of these two windings are comparatively and comprehensively investigated by CFD. Besides, the influence on the thermal performance of the proposed winding of pin spacing in streamwise direction, tilt angle, inlet flow and resistances are discussed. The simulation results show that the maximum temperature of the proposed winding is reduced by 33.2 °C compared with the conventional rectangular winding with the same pure copper conductivity and current input. Two coil prototypes have been manufactured to validate the proposed AM winding concept and CFD models. It shows that even though the resistance of the proposed winding is increased by 26% than the designed value due to the AM challenges, the maximum temperature of the proposed winding can be still reduced by 27.6 °C compared with the rectangular winding. The effectiveness of the proposed winding has demonstrated the great potential of AM technology in improving the machine thermal performance, thus enabling the ever demanding power density requirement to be met for electrified transportation.

REFERENCES

- [1] H. Vella, "Ten Steps to net zero: As the goal to reach net zero in the UK rapidly approaches, we examine Boris Johnson's 10-point plan for a green industrial revolution," *Eng. Technol.*, vol. 16, no. 1, pp. 20-25, Feb. 2021.
- [2] N. Jackson, B. Mecrow, *et al.*, "Electric Machines Roadmap 2020", Advanced Propulsion Centre (APC), Accessed: Feb. 2021, [Online]. Available: https://www.apcuk.co.uk/app/uploads/2021/09/https___www.apcuk_co_uk_app_uploads_2020_11_Technology-Roadmap-Electric-Machines.pdf
- [3] T. Burress, *et al.*, "Electrical Performance, Reliability Analysis, and Characterization", DOE Vehicle Technologies Office Annual Merit Review, USA. Accessed: Jun. 2017. [Online]. Available: https://www.energy.gov/sites/default/files/2017/06/f34/edt087_burress_2017_o.pdf
- [4] F. Yu *et al.*, "Design and multiobjective optimization of a double-stator axial flux SRM with full-pitch winding configuration," *IEEE Trans. Transport. Electric.*, vol. 8, no. 4, pp. 4348-4364, Dec. 2022.
- [5] M. C. Wang, J. Han, Z. Zhang, Y. Hua and H. Gao, "Design and optimization analysis of coreless stator axial-flux permanent magnet in-wheel motor for unmanned ground vehicle," *IEEE Trans. Transport. Electric.*, vol. 8, no. 1, pp. 1053-1062, March 2022.
- [6] R. Burke, A. Giedymis, Z. Wu, H. Chuan, N. Bourne and J. G. Hawley, "A lumped parameter thermal model for single-sided AFPM machines with experimental validation," *IEEE Trans. Transport. Electric.*, vol. 6, no. 3, pp. 1065-1083, Sept. 2020.
- [7] W. Geng, Y. Wang, J. Wang, J. Hou, J. Guo and Z. Zhang, "Comparative study of yokeless stator axial-flux PM machines having fractional slot concentrated and integral slot distributed windings for electric vehicle traction applications," *IEEE Trans. Ind. Electron.*, vol. 70, no. 1, pp. 155-166, Jan. 2023.
- [8] N. Taran, D. Klink, G. Heins, V. Rallabandi, D. Patterson and D. M. Ionel, "A comparative study of yokeless and segmented armature versus single sided axial flux pm machine topologies for electric traction," *IEEE Trans. Ind. Electron.*, vol. 58, no. 1, pp. 325-335, Jan.-Feb. 2022.
- [9] A. S. Fawzal, R. M. Cirstea, K. N. Gyftakis, T. J. Woolmer, M. Dickison and M. Blundell, "Fan performance analysis for rotor cooling of axial flux permanent magnet machines," *IEEE Trans. Ind. Appl.*, vol. 53, no. 4, pp. 3295-3304, July-Aug. 2017.
- [10] P. S. Nasab, R. Perini, A. Di Gerlando, G. M. Foglia and M. Moallem, "Analytical thermal model of natural-convection cooling in axial flux machines," *IEEE Trans. Ind. Electron.*, vol. 67, no. 4, pp. 2711-2721, April 2020.
- [11] A. H. Mohamed, H. Vansompel and P. Sergeant, "An integrated modular motor drive with shared cooling for axial flux motor drives," *IEEE Trans. Ind. Electron.*, vol. 68, no. 11, pp. 10467-10476, Nov. 2021.
- [12] D. Winterborne, N. Stannard, L. Sjöberg and G. Atkinson, "An air-cooled YASA motor for in-wheel electric vehicle applications," *IEEE Trans. Ind. Appl.*, vol. 56, no. 6, pp. 6448-6455, Nov.-Dec. 2020.
- [13] Q. Chen, D. Liang, S. Jia, Q. Ze and Y. Liu, "Analysis of winding MMF and loss for axial flux PMSM with FSCW layout and YASA topology," *IEEE Trans. Ind. Appl.*, vol. 56, no. 3, pp. 2622-2635, May-June 2020.
- [14] B. Zhang, T. Seidler, R. Dierken and M. Doppelbauer, "Development of a yokeless and segmented armature axial flux machine," *IEEE Trans. Ind. Electron.*, vol. 63, no. 4, pp. 2062-2071, Apr. 2016.
- [15] J. Chang, Y. Fan, J. Wu and B. Zhu, "A yokeless and segmented armature axial flux machine with novel cooling system for in-wheel traction applications," *IEEE Trans. Ind. Electron.*, vol. 68, no. 5, pp. 4131-4140, May 2021.
- [16] W. Geng, Z. Zhang and Q. Li, "High torque density fractional-slot concentrated-winding axial-flux permanent-magnet machine with modular SMC stator," *IEEE Trans. Ind. Appl.*, vol. 56, no. 4, pp. 3691-3699, Jul.-Aug. 2020.
- [17] R. Camilleri, D. A. Howey and M. D. McCulloch, "Predicting the temperature and flow distribution in a direct oil-cooled electrical machine with segmented stator," *IEEE Trans. Ind. Electron.*, vol. 63, no. 1, pp. 82-91, Jan. 2016.
- [18] R. Camilleri and M. D. McCulloch, "Integrating a heat sink into concentrated wound coils to improve the current density of an axial flux, direct liquid cooled electrical machine with segmented stator," *Energies*, vol. 14, no. 12, pp. 3619, Jun. 2021.
- [19] J. Zhao, X. Zhang, N. Swaminathan and K. S. Haran, "An overview of high specific power electrical machines and drives technologies for

- electrified aircraft," in *Proc. IEEE Energy Convers. Congr. Expo. (ECCE)*, Oct. 2022, pp. 1-8.
- [20] C. Dong, Y. Qian, Y. Zhang, and W. Zhuge, "A review of thermal designs for improving power density in electrical machines," *IEEE Trans. Transport. Electrific.*, vol. 6, no. 4, pp. 1386-1400, Dec. 2020.
- [21] P. S. Ghahfarokhi, "Opportunities and challenges of utilizing additive manufacturing approaches in thermal management of electrical machines," *IEEE Access*, vol. 9, pp. 36368-36381, Feb. 2021.
- [22] F. Wu and A. M. EL-Refaei, "Toward additively manufactured electrical machines: opportunities and challenges," *IEEE Trans. Ind. Appl.*, vol. 56, no. 2, pp. 1306-1320, Mar.-Apr. 2020.
- [23] R. Wrobel and B. Mecrow, "Additive manufacturing in construction of electrical machines—a review," in *Proc. IEEE Workshop Electr. Mach. Design, Control Diagnosis (WEMDCD)*, Apr. 2019, pp. 15-22.
- [24] M. Gröninger, F. Horsch, A. Kock, M. Jakob and B. Ponick, "Cast coils for electrical machines and their application in automotive and industrial drive systems," in *Proc. 4th Int. Electr. Drives Prod. Conf. (EDPC)*, Sep., 2014, pp. 1-7.
- [25] F. Wu, A. M. EL-Refaei and A. Al-Qarni, "Additively manufactured hollow conductors integrated with heat pipes: design tradeoffs and hardware demonstration," *IEEE Trans. Ind. Appl.*, vol. 57, no. 4, pp. 3632-3642, Jul.-Aug. 2021.
- [26] N. Simpson, G. Yiannakou, H. Felton, J. Robinson, A. Arjunan and P. H. Mellor, "Direct thermal management of windings enabled by additive manufacturing," *IEEE Trans. Ind. Appl.*, early access, 2022.
- [27] J. Pecotich, D. Klink, G. Heins and B. Bahrani, "Additively Manufactured Electric Machine Conductors with Integrated End Turn Heat Exchangers," in *Proc. 25th Int. Conf. Electr. Mach. (ICEM)*, Sep., 2022, pp. 1498-1504.
- [28] D. Goll, D. Schuller, G. Martinek, T. Kunert, J. Schurr, C. Sinz, T. Schubert, T. Bernthaler, H. Riegel, G. Schneider, "Additive manufacturing of soft magnetic materials and components," *Additive Manufacturing*, vol. 27, pp. 428-439 Mar., 2019.
- [29] E. M. H. White, A. G. Kassen, E. Simsek, W. Tang, R. T. Ott and I. E. Anderson, "Net shape processing of alnico magnets by additive manufacturing," in *IEEE Trans. Magn.*, vol. 53, no. 11, pp. 1-6, Nov. 2017.
- [30] W. Sixel, M. Liu, G. Nellis and B. Sarlioglu, "Cooling of windings in electric machines via 3-d printed heat exchanger," *IEEE Trans. Ind. Appl.*, vol. 56, no. 5, pp. 4718-4726, Sept.-Oct. 2020.
- [31] C. Wohlers, P. Juris, S. Kabelac, B. Ponick, "Design and direct liquid cooling of tooth-coil windings," *Electr. Eng.*, vol. 100, no. 4, pp. 2299-2308, Jul. 2018.
- [32] C. A. Rubio-Jimenez, S. G. Kandlikar and A. Hernandez-Guerrero, "Numerical analysis of novel micro pin fin heat sink with variable fin density," *IEEE Trans. Compon. Packag. Manuf. Technol.*, vol. 2, no. 5, pp. 825-833, May 2012.
- [33] B. A. Jaspersen, Y. Jeon, K. T. Turner, F. E. Pfefferkorn and W. Qu, "Comparison of micro-pin-fin and microchannel heat sinks considering thermal-hydraulic performance and manufacturability," *IEEE Trans. Compon. Packag. Technol.*, vol. 33, no. 1, pp. 148-160, Mar. 2010.
- [34] W. A. Khan, J. R. Culham and M. M. Yovanovich, "Optimization of pin-fin heat sinks using entropy generation minimization," *IEEE Trans. Compon. Packag. Technol.*, vol. 28, no. 2, pp. 247-254, Jun. 2005.
- [35] R. Camilleri and M. D. McCulloch, "A new flat winding construction for direct liquid cooled axial flux machine with segmented stators," in *Proc. Int. Conf. Electr. Mach.*, 2018, pp. 2416-2422.
- [36] X. Fan, D. Li, R. Qu, C. Wang and H. Fang, "Water cold plates for efficient cooling: verified on a permanent-magnet machine with concentrated winding," *IEEE Trans. Ind. Electron.*, vol. 67, no. 7, pp. 5325-5336, Jul. 2020.
- [37] R. Wang, X. Fan, D. Li, R. Qu, L. Li and T. Zou, "Convective heat transfer characteristics on end-winding of stator immersed oil-cooled electrical machines for aerospace applications," *IEEE Trans. Transport. Electrific.*, vol. 8, no. 4, pp. 4265-4278, Dec. 2022.
- [38] Y. Gai *et al.*, "Cooling of automotive traction motors: Schemes, examples, and computation methods," *IEEE Trans. Ind. Electron.*, vol. 66, no. 3, pp. 1681-1692, Mar. 2019.
- [39] N. Simpson, R. Wrobel and P. H. Mellor, "Estimation of equivalent thermal parameters of impregnated electrical windings," *IEEE Trans. Ind. Appl.*, vol. 49, no. 6, pp. 2505-2515, Nov.-Dec. 2013.
- [40] Johnson, Kerry, *et al.*, "A copper pyramidal fractal antenna fabricated with green-laser powder bed fusion," *Additive Manufacturing*, vol. 7, pp. 931-941 Feb., 2022.



Hui Tan was born in Jiangxi, China. He received the B.Eng. degree in energy engineering from Changsha University of Science and Technology, Changsha, China, in 2020. He is currently working toward the master's degree in electrical engineering at the Huazhong University of Science and Technology, Wuhan, China. His research interests include the design of permanent magnet machines and cooling design.



Xinggang Fan (Member, IEEE) was born in Hubei, China. He received the B.Eng. degree in energy engineering and the Ph.D. degree in electrical engineering from the Huazhong University of Science and Technology, Wuhan, China, in 2014 and 2019, respectively. He is currently a lecturer with this university. His research interests include electromagnetic-thermal design and analysis of permanent magnet machines, especially those working in the high power density occasions.



Dawei Li (Senior Member, IEEE) was born in China. He received the B.Eng. degrees in electrical engineering from Harbin Institute of Technology, Harbin, China, in 2010, and Ph.D. degree in electrical engineering, from Huazhong University of Science and Technology, Wuhan, China, in 2015. His research interests include design and analysis of novel permanent-magnet brushless machines.



Tianjie Zou (Member, IEEE) received the BEng degree in 2013 and Ph.D. degree in 2018, both in electrical engineering, from Huazhong University of Science and Technology, Wuhan, China. He joined the University of Nottingham, UK, in 2018, as a research fellow within the Power Electronics, Machines and Control (PEMC) Group. In 2020, he was awarded the tenure track Nottingham Research Fellowship and started his independent research career, working towards boosting power density of hundreds kW to MW level electrical machines for automotive traction and aerospace propulsion.

Dr. Zou transitioned to academic role in 2023, and he is currently an Assistant Professor within the Department of Electrical and Electronic Engineering, University of Nottingham. His main research interests include design, analysis, and intelligent control of electric machines, with special attention paid on advanced winding-integration technology in high-speed, high-power PM and reluctance type machines for future electrified transportation. Dr. Zou is the recipient of 2023 Second Prize Best Paper Award from IEEE Transactions on Transportation Electrification.



Wubin Kong (Member, IEEE) was born in Zhejiang, China, in 1986. He received the B.S. and Ph.D. degree in electrical engineering from Zhejiang University, Hangzhou, China in 2009 and 2014, respectively. He is currently a professor with Huazhong University of Science & Technology, Wuhan, China. His research interests include high-power multiphase motor drives and fault-tolerant control motor drive applied in electric vehicles.



Runyu Wang (Student Member, IEEE) was born in Anhui, China. He received the B.Eng. degree in electrical engineering and automation from Anhui University, Hefei, China, in 2019. He is currently working toward the Ph.D. degree in Huazhong University of Science and Technology, Wuhan, China. His research interests include electromagnetic and cooling design of high power density permanent magnet fault tolerant machines.



Xiaoxue Chen was born in China. She received the B.E.E. in electrical engineering from Harbin Institute of Technology, Harbin, China, in 2010, and M.S.E.E. degrees in the School of Electrical and Electronic Engineering, Huazhong University of Science and Technology, Wuhan, China, in 2016. Her research interests include design and analysis of power system.



Ronghai Qu (Fellow, IEEE) was born in China. He received the B.E.E. and M.S.E.E. degrees from Tsinghua University, Beijing, China, in 1993 and 1996, respectively, and the Ph.D. degree from the University of Wisconsin-Madison, in 2002, all in electrical engineering.

In 1998, he joined the Wisconsin Electric Machines and Power Electronics Consortiums as Research Assistant. He became a Senior Electrical Engineer with Northland, a Scott Fetzer Company in 2002. Since 2003, he had been with the General Electric (GE) Global Research Center, Niskayuna, NY, as a Senior Electrical Engineer with the Electrical Machines and Drives Laboratory. From 2010, he has been a professor with Huazhong University of Science & Technology, Wuhan, China. He has authored over 260 published technical papers and is the holder of over 80 patents/patent applications.